Title

Characterization and operation optimization of large aperture optical interferometers using binary pseudorandom array test standards

ISBN

9781510620698

Authors

Yashchuk, Valeriy V
Babin, Sergey
Cabrini, Stefano
et al.

Publication Date

2018-08-18

DOI

10.1117/12.2322011

Peer reviewed

Characterization and operation optimization of large aperture optical interferometers using binary pseudorandom array test standards

Valeriy V. Yashchuk,[*,a] Sergey Babin,[b] Stefano Cabrini,[c] Ulf Griesmann,[d] Ian Lacey,[a] Keiko Munechika,[b] Carlos Pina Hernandez,[b] and Quandou Wang[e]

[a]Advanced Light Source Berkeley, Lawrence Berkeley National Laboratory, California 94720, USA; [b]aBeam Technologies, Inc., Hayward, California 94541, USA; [c]Molecular Foundry, Lawrence Berkeley National Laboratory, California, 94720, USA; [d]Engineering Physics Division, National Institute of Standards & Technology, Gaithersburg, Maryland 20899, USA; [e]ASPAC Technologies LLC, 2440 140th Ave. Ne Unit48, Bellevue, WA 98005, USA

ABSTRACT

Recently, a technique for calibration of the Modulation Transfer Function (MTF) of a broad variety of metrology instrumentation has been established. The technique is based on test samples structured according to binary pseudo-random (BPR) one-dimensional sequences and two-dimensional arrays. The inherent power spectral density of BPR gratings and arrays, has a deterministic white-noise-like character that allows a direct determination of the MTF with a uniform sensitivity over the entire spatial frequency range and field-of-view of an instrument. As such, the BPR samples satisfy the characteristics of a test standard: functionality, ease of specification and fabrication, reproducibility, and low sensitivity to manufacturing error. Here we discuss our recent developments working with support of the U.S. Department of Energy on industrialization of the technique. The goal is to develop affordable BPR test samples, application procedures, and data processing software, suitable for thorough characterization of optical interferometers and microscopes, as well as x-ray, electron (scanning and transmission), and atomic force microscopes. We report on the development of BPR array test samples optimized for advanced characterization (including the instrumental MTF and aberrations) and operation optimization of large aperture optical interferometers. We describe the sample fabrication process and tests to verify the compliance to desired surface topography. The data acquisition and analysis procedures for application of the technique for precise focusing of Fizeau interferometer are discussed in detail.

Keywords: calibration, modulation transfer function, power spectral density, Fizeau interferometers, binary pseudorandom, test standard, aberration, surface metrology

1. INTRODUCTION

Recently, a technique for calibration of the modulation transfer function (MTF) of a broad variety of metrology instrumentation has been established (see, for example, Refs. [1-5] and references therein). The technique is based on test samples structured according to binary pseudo-random (BPR) one-dimensional sequences and two-dimensional arrays. The inherent power spectral density of BPR gratings (BPRGs) and arrays (BPRAs) has a deterministic white-noise-like character that allows a direct determination of the squared MTF with a uniform sensitivity over the entire spatial frequency range and field-of-view of an instrument. As such, the BPR samples satisfy the characteristics of a test standard: functionality, ease of specification and fabrication, reproducibility, and low sensitivity to manufacturing error.

Here, we discuss the development of BPR array test samples suitable for advanced characterization and operation optimization of large aperture optical interferometers, including the instrumental MTF and aberrations. Two kinds of BPRA sample were evaluated. One was fabricated on a very flat silicon surface, the other on low-cost substrates made from a borosilicate glass. The two types of substrate have significantly different surface quality and the BPRA samples tested in this work have drastically different quality of the BPRA patterns. Nevertheless, using the original data acquisition and analysis algorithms and procedures described in this report, it become possible to characterize the performance of a Fizeau interferometer using both types of samples and to use them for precise focusing of the interferometer.

*vvyashchuk@lbl.gov; phone 1 510 495-2592; fax 1 510 486-7696; lbl.gov

2. EXPERIMENTAL SETUP

The measurements discussed throughout the present paper were performed at the Advanced Light Source (ALS) X-Ray Optics Laboratory (XROL) [6,7]. The experimental setup of a 6 inch (152 mm) aperture Fizeau interferometer in the XROL clean-room is depicted in Fig. 1. The optical table with the interferometer is located inside a hutch that is surrounded with a plastic curtain system. The advanced environmental conditions in the lab together with the double insulation with the hutch and curtain provides stable ambient temperature and humidity around the interferometer, and, as a result, a high repeatability of the interferometric measurements is achieved.

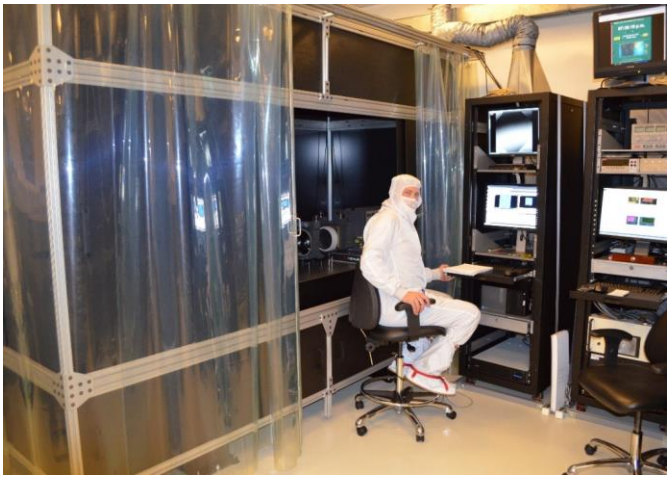

Figure 1. Measurement setup of a commercial Fizeau interferometer in the XROL clean-room.

Figure 2 shows the experimental setup with the LBNL BPRA sample placed in the front of the interferometer. For the sample holding and alignment, we use a precision tilting stage. The stage has a sample mount with three pins for holding the sample without stress. Each pin is machined with a cone stop at the edge that helps to limit and fix the position of the sample front surface with respect to the interferometer. The interferometer focus setting is adjusted stepwise with a remote control pad. A transmission flat with a peak-to-valley flatness error of better than $\lambda/50$ is mounted in the interferometer.

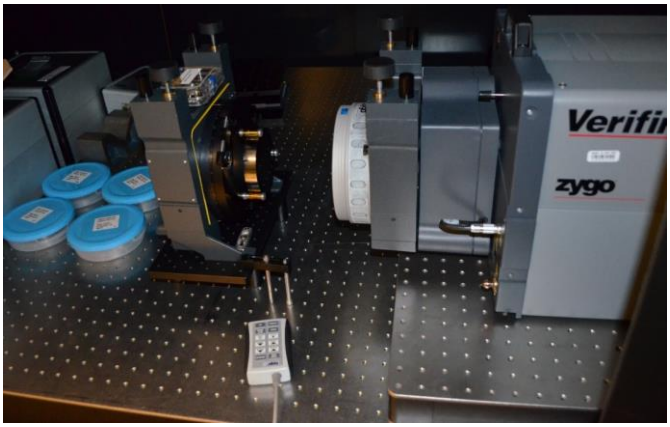

Figure 2. Experimental setup with the LBNL BPRA sample mounted in the precision tilting stage and placed in the front of the interferometer. The NIST samples are stored in the plastic containers with blue caps. The interferometer remote control pad is used for adjustment of the focus distance.

The repeatability of the measurements is illustrated in Fig. 3 with an example of the LBNL BPRA sample. In spite of the rough surface of the sample due to the BPRA structure, the root-mean-square (RMS) variation of the difference of two measurements, each consisting of 4 averaged measurements, performed with a time interval of about 10 min is 0.41 nm.

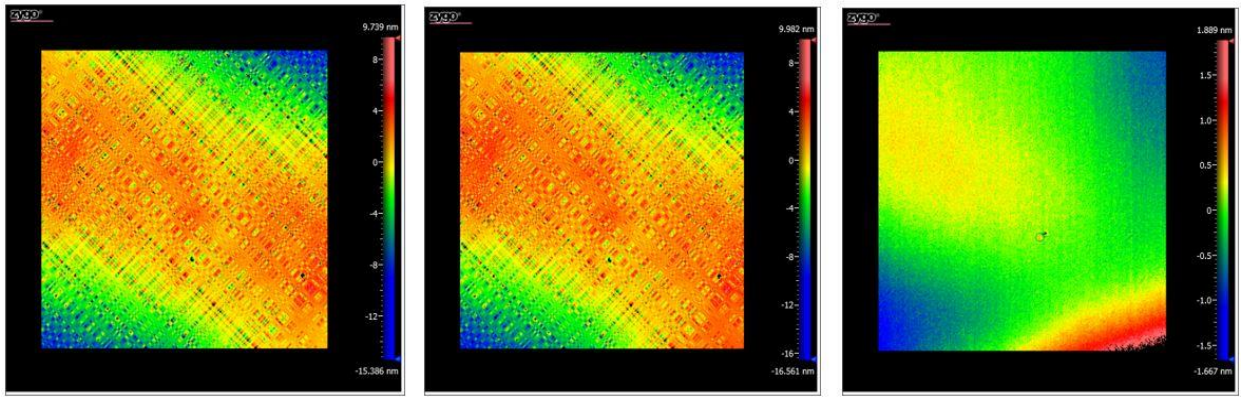

Figure 3. Surface height distributions of the LBNL BPRA sample recorded in two identical measurements (the left-hand and central images) and the difference of the measurements. The surface height distributions are shown after detrending with the best fit plane surface (the piston and tilt detrending). The RMS variations of the height distributions are 2.87 nm, 3.09 nm, and 0.41 nm (from left to right).

The field-of-view of the Fizeau interferometer at the XROL has a diameter of 6 inches. At the maximum magnification of around four, the effective pixel size limiting the lateral resolution is about 40 µm. The design of the LBNL sample is based on a BPR array [8,9] consisting of 4127 × 4129 square elements [2] with the fundamental element dimension of 15 µm so that the squared instrumental MTF can be characterized over the entire dynamic range of the interferometer. The total area of the sample is 61.935 mm × 61.905 mm^2, and the step height is about 60 nm.

Such a sample satisfies the major requirements for a suitable MTF test sample. The lateral size of the smallest feature (the BPRA fundamental size) is smaller by a factor of three than the interferometer lateral resolution at the largest magnification. The height of the BPRA structure is much smaller than the wavelength of the interferometer light of 633 nm. Additionally, for the LBNL sample fabrication, we required the BPRA structure height to be significantly larger than the peak-to-valley surface height variation of the sample substrate at the higher spatial frequencies that cannot be detrended by the interferometer's data processing software. The later condition makes the analysis of the data measured with the sample more straightforward.

In the case of the LBNL sample, the BPRA structure was patterned in a chromium layer on the surface of a super polished crystalline silicon substrate with 100 mm diameter and 19 mm thickness using a lift-off process. The back side of the substrate was also optically polished and coated with a layer of chromium to decrease the likelihood of deforming the substrate due to the surface tension of the BPRA structure.

Another set of BPRA standards was fabricated at NIST on double-side polished low-cost borosilicate glass substrates with 100 mm diameter and 12.5 mm thickness. A maskless photolithography system was used to pattern a chromium layer on the substrate with a 3167 x 3169 element BPR array that has 20 µm wide square elements [8,9] using a lithographic lift-off process. After resist processing the patterned chromium layer was used as a hard mask to etch the BPR array into the glass using a reactive ion etching process. Samples with different step heights were fabricated, and some of the finished samples were coated with gold. The gold-coated BPRA sample used in the investigations described in the present paper has the step height of about 50 nm.

3. OPTIMIZATION OF THE FOCUS SETTING IN MEASUREMENTS WITH THE LBNL BPRA SAMPLES

The goal of our measurements with the LBNL BPRA sample was to find the optimal focus setting for the experimental arrangement shown in Fig. 2 that can be used for surface metrology with other optics of interest.

The idea of the optimization consists of comparison of the power spectral densities (PSDs) of the sample height distributions recorded at different adjustments of the focus setting. The PSD with the largest amplitude at the higher spatial frequencies corresponds to the optimal setting. In other words, the procedure allows adjusting the interferometer to the maximum possible spatial resolution determined by the inherent squared MTF of the instrument.

Analogous approach was recently applied for precision focusing of an x-ray microscope [4] with using a specially developed BPR multilayer test sample [5].

A numerical measure of dependence of the interferometer performance on the focus setting could be the integral of the entire PSD that has the physical (statistical) meaning of the variance, or the square of the RMS variation of the surface height distribution. In order to make the criterion more sensitive to the focus adjustment, the integration can be performed over the higher spatial frequency range, covering the frequency range before and after the resolution-limited roll-off in the measured PSD.

3.1 Measurements with the LBNL BPRA sample aligned parallel to the pixel pattern of the interferometer's CCD camera

Figure 4 reproduces the intensity fringe images of the LBNL BPRA sample recorded at the visually-optimized setting obtained after a focus adjustment of 300 steps of the interferometer's focus adjustment motor counted out from the lowest focus setting (the left-hand image) and at a setting with visually noticeable defocus obtained after a 350-step focus adjustment (the right-hand image). The corresponding height distributions are shown in Fig. 5.

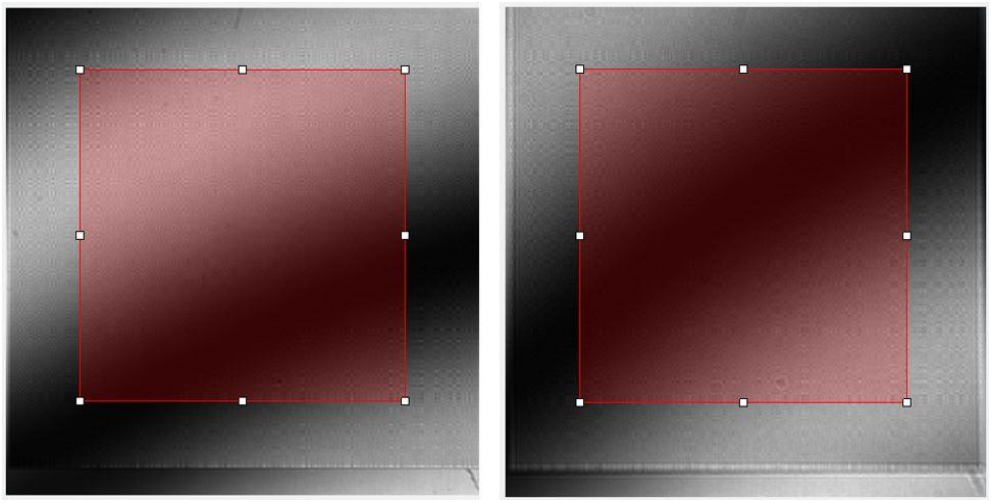

Figure 4. Intensity fringe images of the LBNL BPRA sample recorded by the Fizeau interferometer with different focus settings: (the left-hand image) at the visually-optimized setting obtained after 300-step adjustment, and (the right-hand image) at the setting with visual defocus obtained after 350-step adjustment from the lowest focus setting. The better focus for the left image is indicated by the decreased blurring of the bottom edge of the BPRA structure.

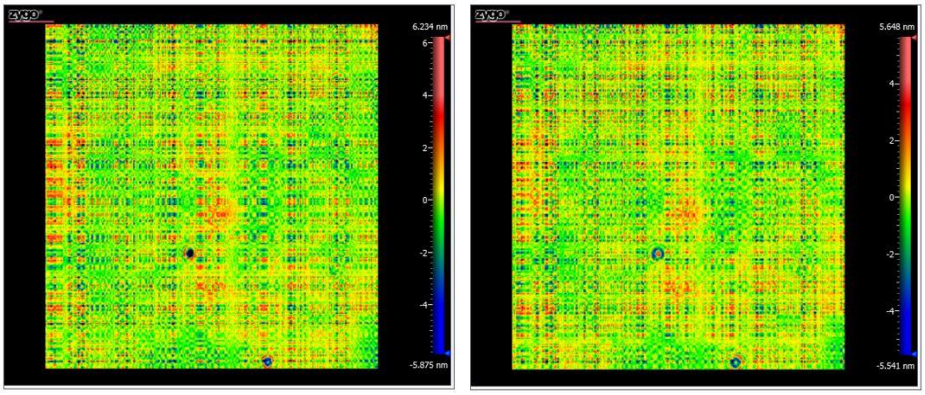

Figure 5. Surface height distributions of the LBNL BPRA sample recorded at different focus settings: (the left-hand image) at the visually-optimized setting obtained after the 300-step adjustment, and (the right-hand image) at the setting with visual defocus obtained after 350-step adjustment from the lowest focus setting. The surface height distributions are shown after detrending with the first four Zernike polynomials (see discussion in the text). The RMS variations of the height distributions are 1.3048 nm and 1.3062 nm, respectively.

For the measurements, the zoom factor was selected to be about 2, providing the effective pixel size of the images of about 70 µm. The size of the mask seen in Fig. 4 and used for data analysis is 680 × 680 pixels.[2]

Despite the difference in focusing quality that can be clearly seen in Fig. 4, the sharpness of the BPRA structure in the corresponding measured height distributions in Fig. 5 is not visually distinguishable. The values of the RMS height variation are also almost the same at 1.3048 nm for the left and 1.3062 nm for the right image in Fig. 5. As we show in the next section (Sec. 3.1), the visually-optimized focus setting is still far from the real optimum, which explains the nearly identical height measurements.

Surface height measurements of the BPRA structure on the super-polished substrate contain a very low spatial frequency component that is not intrinsic to the test sample but is due to the flatness error of the interferometer transmission flat, and, to some degree, residual interferometer errors. Lower spatial frequency variation of the measured height distributions were removed with best-fit Zernike polynomials describing piston, tilt, power, astigmatism, and coma aberrations. The effect of the detrending is illustrated in Fig. 6, where the measurement at the visually-optimized focus setting (Fig. 5) is depicted as detrended (the left-hand image) with the best-fit plane surface and (the right-hand image) with a model including Zernike polynomials up to coma terms.

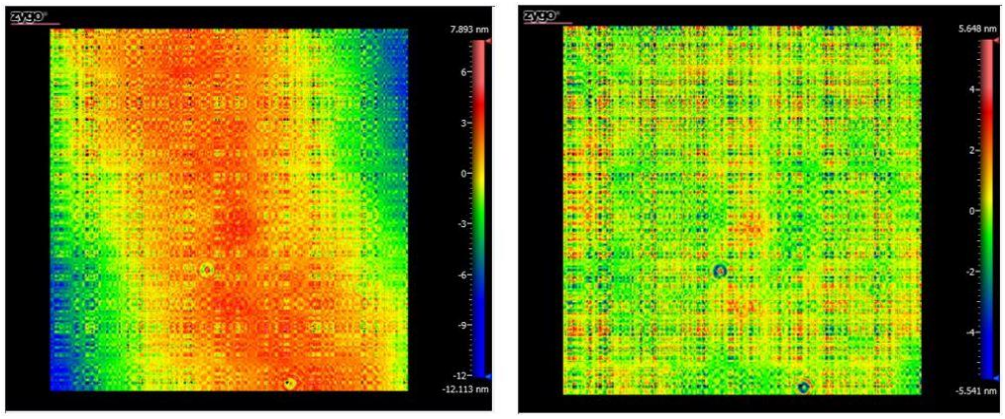

Figure 6. Surface height distribution of the LBNL BPRA sample corresponding to the same measurement at the visually-optimized focus setting, but with different detrending: (the left-hand image) with the best-fit plane surface and (the right-hand image) with Zernike polynomials describing piston, tilt, power, astigmatism, and coma aberrations.

In the case of images depicted in Fig. 4 and 5, a hint to an improvement of the focusing can be seen when comparing the one-dimensional (1D) PSD spectra along the horizontal axis shown in Fig. 7.

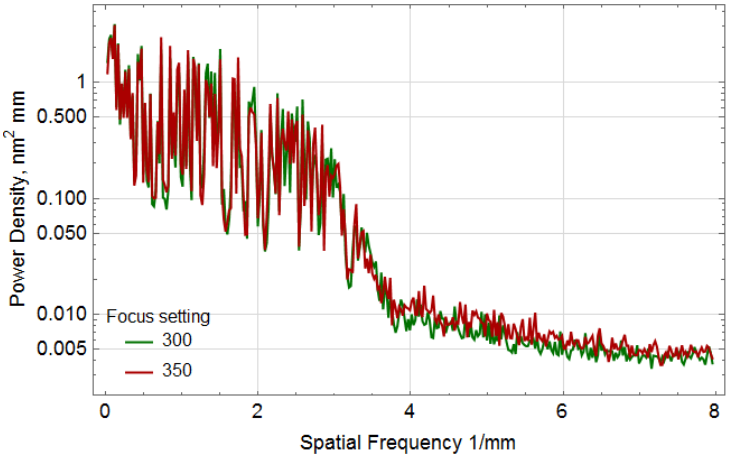

Figure 7. 1D PSD spectra in the horizontal direction of the LBNL BPRA sample calculated for the surface height distributions in Fig. 5, recorded at different focus settings: (the green line) at the visually-optimized setting obtained after 300-step adjustment, and (the red line) at the setting with visual defocus obtained after 350-step adjustment from the lowest focus setting.

The roll-off of the PSD spectrum corresponding to the visual focusing is slightly offset towards higher frequencies. This observation supports the idea that the dependence of the PSD on the focus setting can be used for tuning of the interferometer focus setting. However, it also becomes evident that a limiting factor of the adjustment is the larger amplitude of variation of the 1D PSD spectra.

We think that the observed strong variation is mostly due to the large difference, by a factor of approximately 5, between the effective pixel size of the interferometer (70 μm) and the minimum feature size of the BPRA sample (15 μm), whereas the optimal ratio is about 2. In this case, the lower spatial frequency pattern of the BPRA mostly contributes to the measurements. But this pattern, when shortened, has a strong autocorrelation, leading to the observed variation of the PSD.

We have carried out measurements similar to those discussed above, but at the maximum zoom factor of the interferometer to test the explanation and the result is shown in Fig. 8. Indeed, the 1D PSD spectra for these measurements are noticeably smoother. However, the sensitivity to the change of the resolution is not improved. This can be thought of as an indication of a strong auto-correlation of the measured BPRA area.

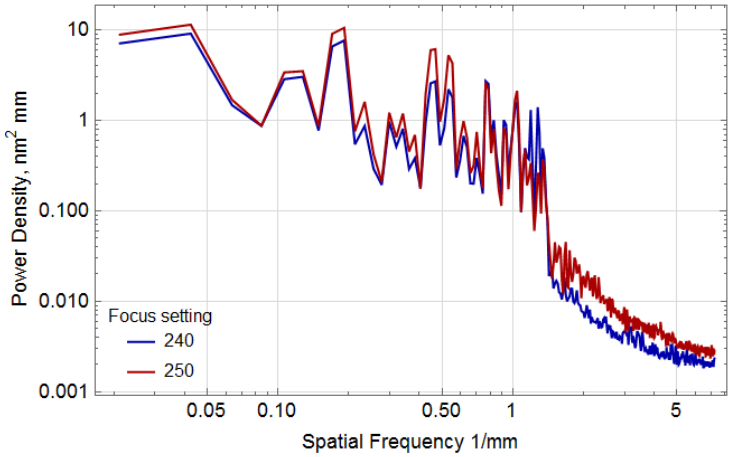

Figure 8. 1D PSD spectra in the horizontal direction of the LBNL BPRA sample calculated for the surface height distributions recorded at the maximum zoom of the interferometer at two different focus settings: at the optimized setting of 250 steps (the upper red line), and at the setting of 240 steps (the lower blue line), much closer to the focus than in Fig. 7.

For precision optimization of the focus setting, even for significantly lower zoom, we suggest and demonstrate a simple and efficient method for obtaining very smooth 1D PSD of the high-resolution BPRA sample, as the LBNL one, in the following subsection.

3.2 Measurements with the LBNL BPRA sample rotated by approximately 45 degrees

As discussed above, the strong variation of the 1D PSD spectrum measured with the BPRA sample oriented parallel to the interferometer CCD pixel structure is due to the lower spatial frequency autocorrelation of the shortened BPRA pattern along the axis of the sample grid. The autocorrelation can be decreased when the sample is rotated by approximately 45 degrees with respect to the pixel pattern of the CCD, which effectively increases the element size of the BPRA sample along the axis of the interferometer CCD camera. The intensity fringe images of the rotated sample, recorded at the focus settings of 240 steps and 251 steps, are shown in Fig. 9. Figures 10 and 11 show the corresponding height and PSD distributions, respectively.

As expected, the PSD spectra of the rotated sample in Fig. 11 are much smoother (compare with Fig. 7).

Moreover, even though the sharpness of the BPRA structure in the corresponding height distributions in Fig. 10 is visually indistinguishable, the PSDs are clearly different at a focus adjustment difference of only 10 steps. The spectrum recorded at the 251-step focus adjustment has the resolution roll-off at higher spatial frequency. The PSD corresponding to stronger defocusing has a characteristic high spatial frequency bump after the Nyquist frequency. This can be thought of as a signature of the squared MTF of a measurement with oversampling, when the effective pixel size of the interferometer is much smaller when the instrumental resolution.

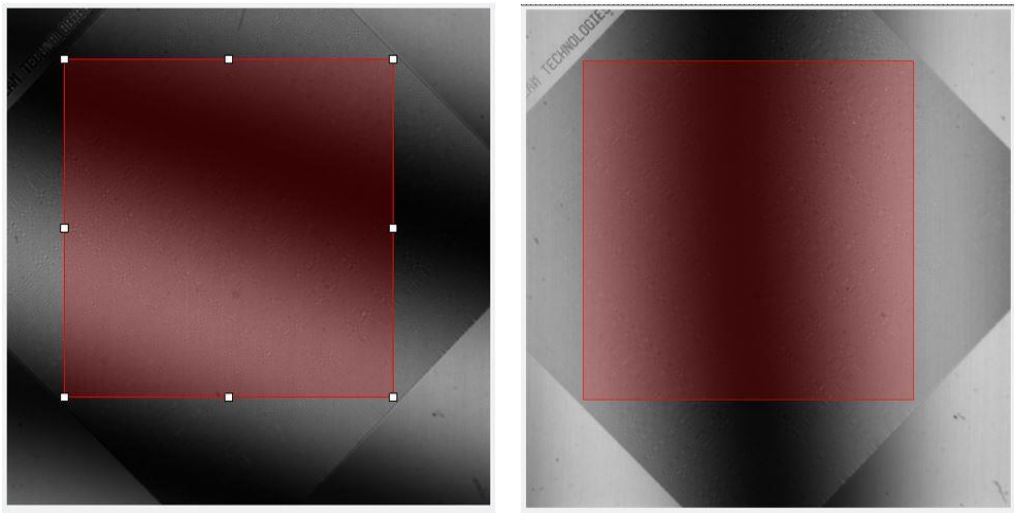

Figure 9. Intensity fringe images of the LBNL BPRA sample rotated by approximately 45 degrees as recorded with the Fizeau interferometer at the focus setting of 240 and 251 steps, the right and left images, respectively. The red squares show the mask selecting the surface area of 680 × 680 pixels^2 used for data analysis.

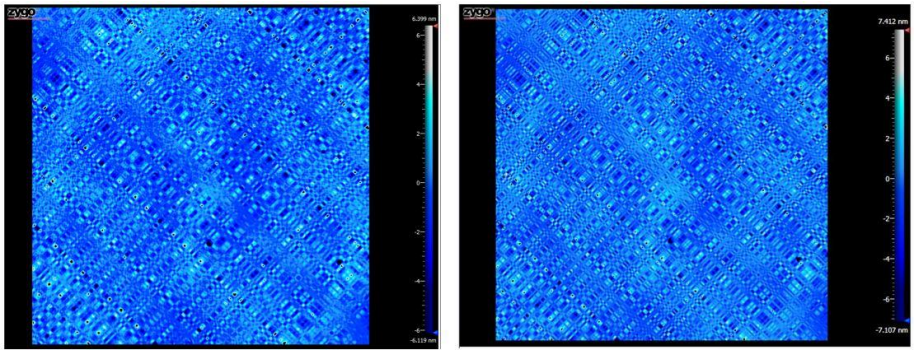

Figure 10. Surface height distributions of the LBNL BPRA sample rotated by approximately 45 degrees as recorded at different focus settings: 240 steps and 251 steps the right and left images, respectively. The surface height distributions are shown after detrending with the Zernike polynomials describing piston, tilt, power, astigmatism, and coma. The RMS variations of the height distributions are 1.37806 nm and 1.3062 nm, respectively.

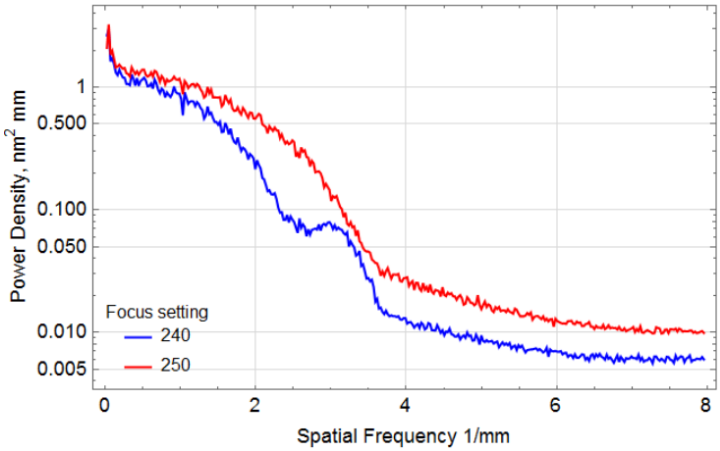

Figure 11. 1D PSD spectra in the CCD horizontal direction calculated for the surface height distributions (Fig. 10) of the rotated LBNL BPRA sample using the interferometer point source mode at two focal adjustments, 240 steps (blue) and 251 steps (red).

The dependence of the PSDs in the vicinity of the roll-off on the focus adjustment is illustrated in Fig. 12. A numerical measure of the corresponding dependence of the interferometer performance on the focus setting is the variance of the surface height distribution equal to the integral of the 1D PSD. For the measurements in Fig. 12, the variance of the surface height distribution changes by a factor of more than 1.5, as depicted in the table in Fig. 12.

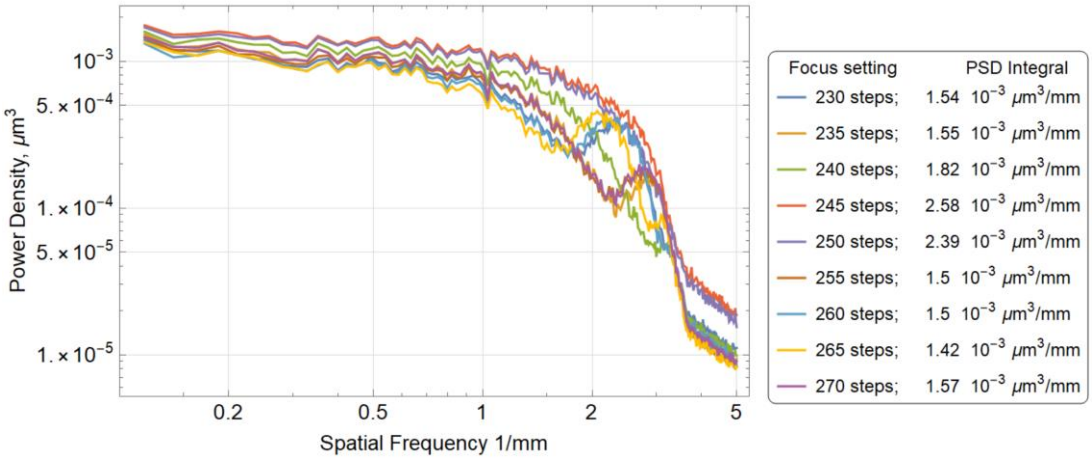

Figure 12. 1D PSD spectra in the CCD horizontal direction of the rotated LBNL BPRA sample measured using the Fizeau interferometer under test in the point source mode at different focal adjustments between 230 steps and 270 steps.

The sensitivity of the PSDs measured with the rotated BPRA to the focus adjustment is demonstrated in Fig. 13, where one can see that the optimal focus adjustment is between the steps 251 and 252. The resolution of the focus adjustment (possible with the instrument's remote control) is not enough to more precisely optimize the focal distance in the measurements with the interferometer in the point source mode.

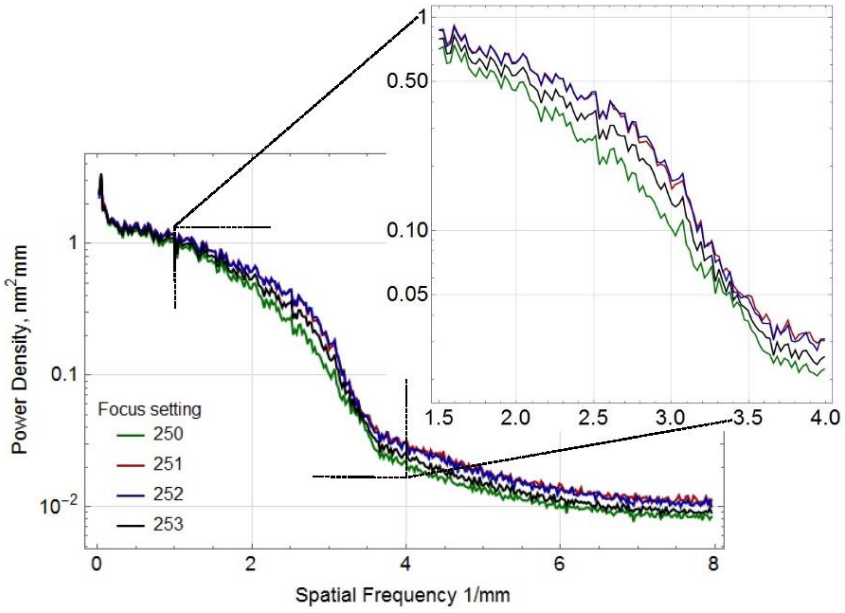

Figure 13. 1D PSD spectra in the CCD horizontal direction of the rotated LBNL BPRA sample measured using the Fizeau interferometer under test in the point source mode at the vicinity of the optimal focal adjustments with 1-step increment.

Figure 14 summarizes the observations when optimizing the focus of the Fizeau interferometer with the LBNL BPRA sample. It shows the PSD spectra measured with the BPRA substrate at focal setting 251 using point source mode with the substrate oriented parallel to the detector (blue), using point source mode with the substrate rotated by 45 degrees (red), and using the extended source mode with the substrate rotated by 45 degrees (green).

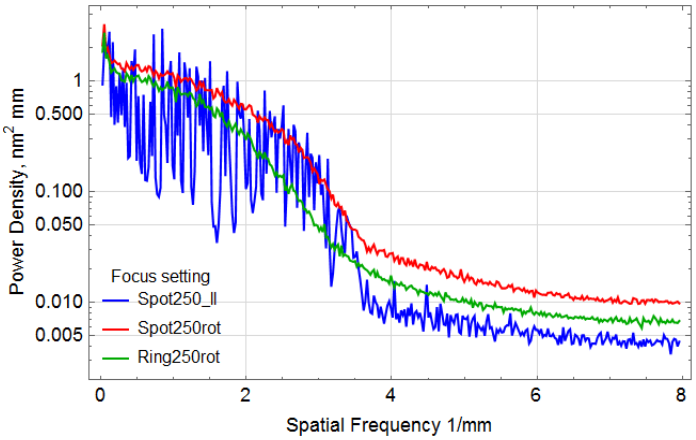

Figure 14. The PSD spectra measured with the BPRA substrate at near the optimal focus using the interferometer's point source mode with the substrate oriented parallel to the detector (the blue line), point source mode with the substrate rotated by 45 degrees (the red line), and Ring mode with the substrate rotated by 45 degrees (the green line).

As expected, the resolution roll-off measured in the point source mode with rotated and unrotated sample occurs at the same spatial frequencies. The resolution in the extended source mode is noticeably lower.

There is one more interesting observation that requires a solid explanation in future work. This is the change of the high frequency background depending on the focal setting (Figs. 12-14), on the sample orientation, and on the interferometer's mode of operation.

4. MEASUREMENTS WITH THE NIST GOLD COATED BPRA SAMPLES

4.1 Measurements with the NIST BPRA sample aligned parallel with the pixel pattern of the interferometer's CCD camera

Figure 15 depicts a measurement of the gold coated BPRA sample fabricated at NIST with the Fizeau interferometer available at the ALS XROL.

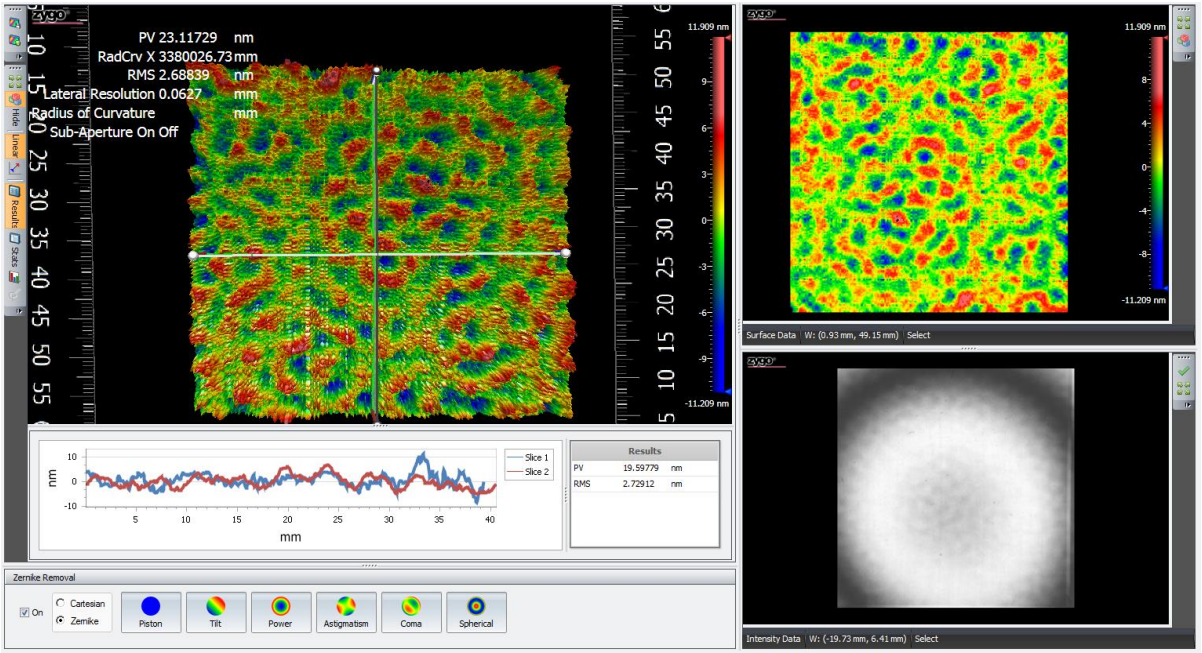

Figure 15. Printout of a measurement of the NIST gold coated BPRA sample with the Fizeau interferometer under test.

The sample image was aligned parallel to the pixel pattern of the interferometer's CCD camera. The measurement was performed in the point source mode at the near optimal focus obtained during the measurements with the LBNL sample. A pronounced mid-spatial frequency pattern on the surfaces of the low-cost substrate used for the sample fabrication makes the BPRA structure etched into the substrate surface almost invisible.

The PSD spectra measured in point and extended source modes are shown in Fig. 16. The spectra are nearly identical. Note that the strong variation of the spectra is similar to that of the LBNL sample in Fig. 7.

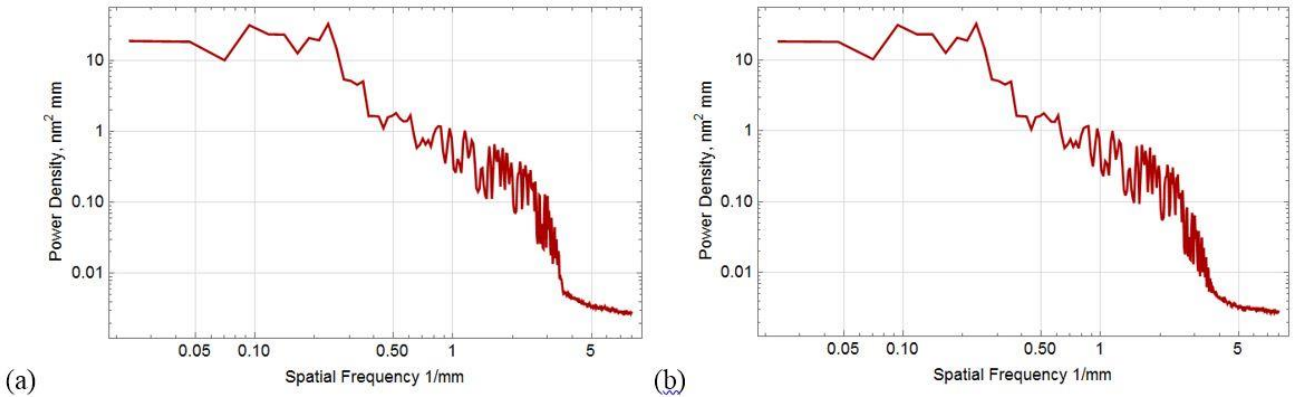

Figure 16. The PSD spectra measured in the interferometer's (a) Point source and (b) extended source modes with the NIST gold coated BPRA sample aligned parallel to the pixel pattern of the interferometer's CCD camera.

A noticeable difference of the PSDs measured with the NIST and LBNL sample are the middle frequency bumps in the PSDs of the NIST sample. These bumps are obviously caused by the surface height imperfection of the substrate with the amplitude comparable to the height of the etched BPRA structure. However, while the polishing imperfection affects mid-spatial frequencies, the PSD spectrum of the NIST sample correctly reproduces the instrument's resolution roll-off at higher spatial frequencies. This makes the sample still useful for some test with the interferometer, such as the focus optimization discussed in the next section.

4.2 Measurements with the NIST BPRA sample rotated by approximately 45 degrees

Following to the method suggested in Sec. 3.2 for decreasing the variations in the measured PSDs by rotating the sample, we have performed a series of measurements with the NIST sample rotated by approximately 45 degrees with respect to the pixel pattern of the CCD.

The intensity fringe image of the rotated NIST sample and the corresponding surface height distribution recorded near the optimal focus are shown in Fig. 17.

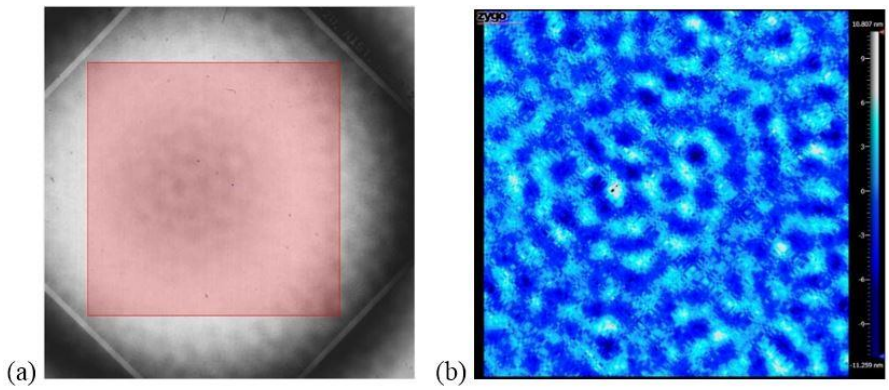

Figure 17. (a) Intensity fringe image and (b) the surface height distribution of the NIST BPRA sample rotated by approximately 45 degrees as recorded with the Fizeau interferometer near the optimal focus. The red square in the intensity image shows the mask selecting the surface area of 680 × 680 pixels used for data analysis. The surface height distribution is the result of detrending the measured distribution with the Zernike polynomials accounting for the piston, tilt, power, astigmatism, coma, and spherical shape.

As in the measurement with parallel alignment, in the measurements with the rotated NIST sample the strong mid-spatial frequency pattern of the substrate surface renders the etched BPRA structure nearly invisible.

Figure 18 shows the PSD spectra measured with the rotated NIST sample at three focus adjustments different by one step from the found optimum.

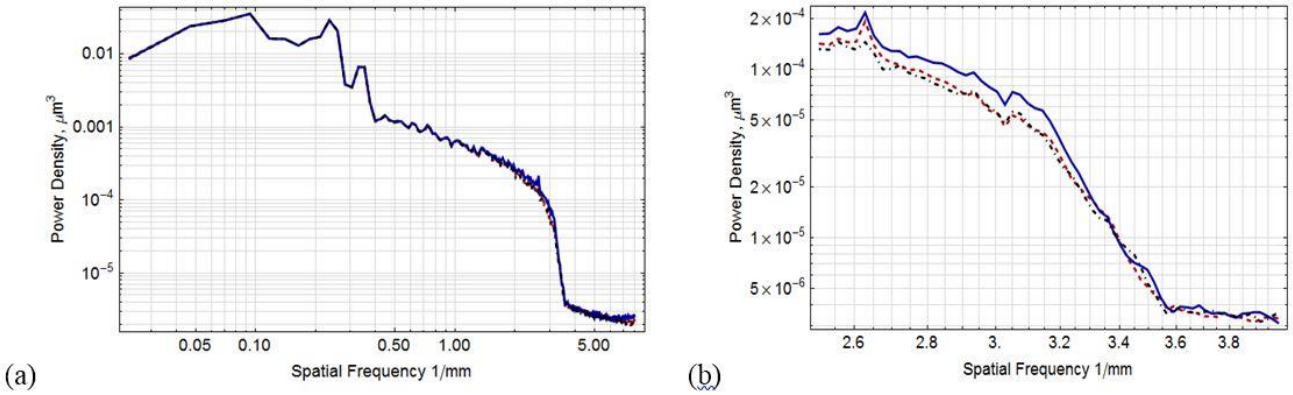

Figure 18. (a) 1D PSD spectra of the rotated NIST gold coated BPRA sample measured using the Fizeau interferometer under test in the point source mode at the vicinity of the optimal focal adjustments with 1-step increment; (b) the near roll-off area of the PSDs shown with enlarged scale.

As before, the PSD spectra of the rotated NIST sample in Fig. 18 are much smoother (compare with Fig. 16). Moreover, despite the BPRA structure in the corresponding height distributions (see Fig. 17) is almost invisible, the PSDs are clearly different at the focus adjustments altered by only 1 step. This proves the usefulness of the sample in such applications as focus optimization of large aperture Fizeau interferometers.

5. APPLICATION OF THE DEVELOPED METHOD FOR FOCUS OPTIMIZATION TO THE MEASUREMENTS WITH AN OPTICAL GLASS SUBSTRATE WITH AN EXTREMELY CURVED SURFACE PROFILE

Figure 19 illustrates the power of the developed method with an example of measurements with the Fizeau interferometer available at the ALS XROL of an optical glass substrate with a strongly curved surface profile.

The profile measured at the focus adjusted with a technique recommended by the interferometer vendor is shown in Fig. 19a. In this case, due to the limitation of the focusing procedure, the most curved central part of the surface profile is not recovered (the black ring in the right plot of Fig. 19a).

Application of our focusing procedure that is free of the subjectivity inherent to the standard technique allows reliable measurements over the entire profile of the optical substrate under test – Fig. 19b.

6. CONCLUSIONS

We have suggested and demonstrated an original method for high precision focus tuning of large aperture optical Fizeau interferometers. The idea of the method is to adjust the interferometer to the maximum possible spatial resolution measured as the higher spatial frequency cut-off of the inherent modulation transfer function of the instrument. Practically, we compare the power spectral densities of a specially developed BPRA test sample recorded at different adjustments of the focus setting. The 1D PSD with the largest amplitude at the higher spatial frequencies corresponds to the optimal setting.

We have described two realizations of the method when using two BPRA samples of significantly different quality and, correspondingly, the cost. We have experimentally demonstrated that in application to optimal focusing of the interferometer, the both samples have the same performance.

In application of the method to the Fizeau interferometer available at the ALS XROL, we have experimentally demonstrated that the sensitivity of the method is better than the available resolution of the focus adjustment. In order to

get the maximum sensitivity, the BPRA samples have to be rotated with respect to the pixel grid of the interferometer's CCD detector.

A numerical measure of dependence of the interferometer performance on the focus setting could be the integral of the entire PSD that has the physical (statistical) meaning of the variance, or the square of the RMS variation of the surface height distribution. In order to make the criterion more sensitive to the focus adjustment, the integration can be performed over the higher spatial frequency range, covering the frequency range before and after the resolution-limited roll-off in the measured PSD.

Note that an additional improvement of the PSD measurements of BPRA structure on a low quality substrate can be achieved by subtracting the reference PSD of the polished substrate measured before fabrication of the BPRA structure. Because the BPRA structure does not correlate with the pattern of the substrate surface imperfections, the corrected PSD is expected to be mostly due to the BPRA structure. As the result, the PSD at the higher (around the Nyquist) and middle frequencies has to be much cleaner. Of course, it can still be a difference at the lower spatial frequencies due to the stress produced by the coating. But in the calibration of the squared instrumental MTF, this distortion can be ignored. The corresponding tests are in progress.

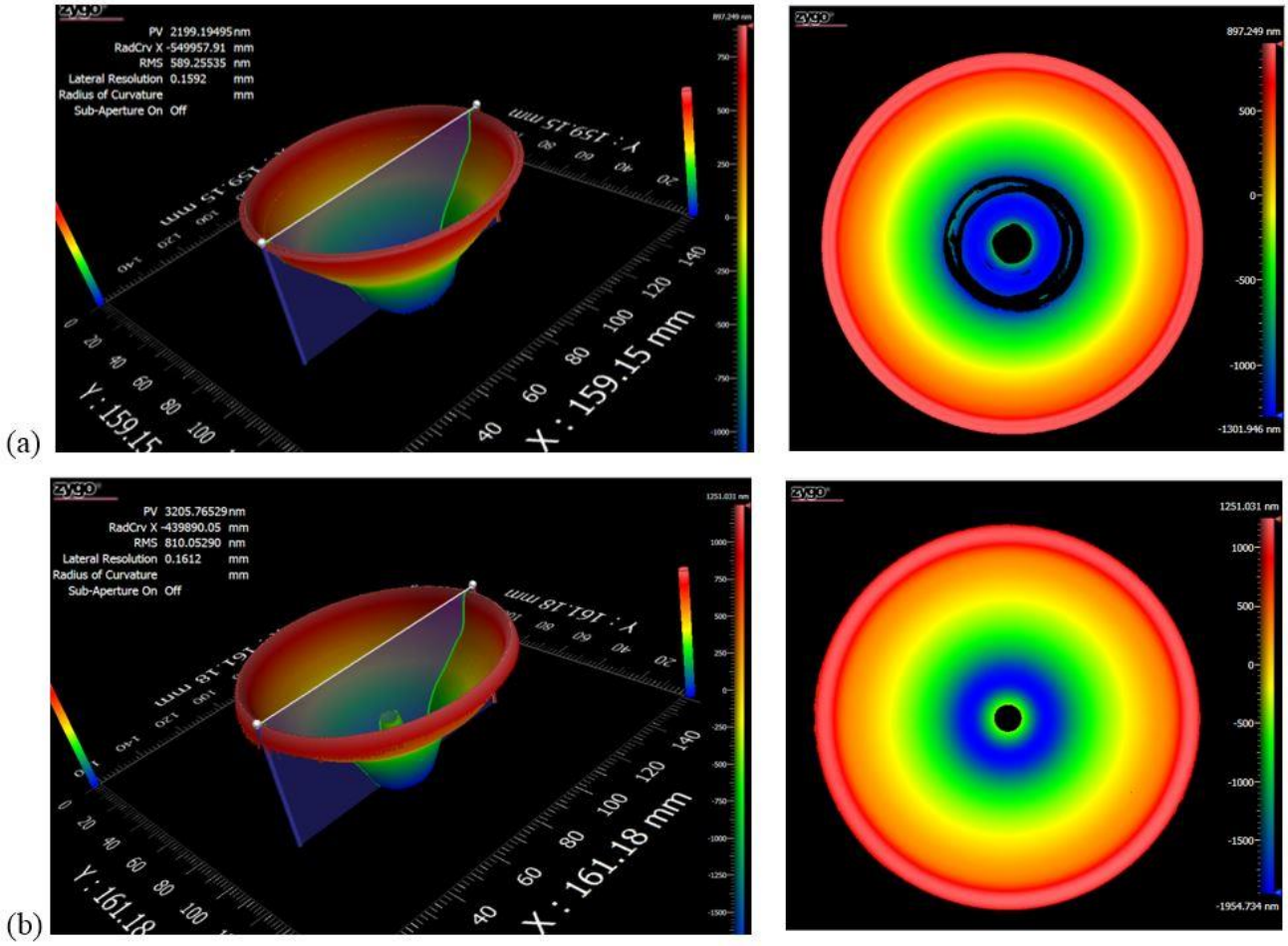

Figure 19. Measurement with the Fizeau interferometer available at the ALS of an optical glass substrate with extremely curved surface profile at the interferometer's focus adjusted using (a) the technique recommended by the vendor and (b) the method suggested and discussed in this paper.

ACKNOWLEDGEMENTS

The authors are thankful to Danielle Bechtold, Rob Bechtold, and Dave Mohring from OptiPro Systems, Inc. for providing the optical glass substrate with a strongly curved surface profile. This work was supported by the U.S. Department of Energy Office of Science, Office of Basic Energy Sciences, and Small Business Technology Transfer (STTR) programs under Award Numbers DE-SC0011352. Research at the Advanced Light Source and the Molecular Foundry at Lawrence Berkeley National Laboratory is supported by the Office of Science, Office of Basic Energy Sciences, and Material Science Division of the U.S. Department of Energy under Contract No. DE-AC02-05CH11231. The BPRA mirrors on glass substrates were fabricated with the help of tools and resources available at the NIST Center for Nanoscale Science and Technology (CNST).

REFERENCES

[1] V. V Yashchuk, W. R McKinney, P. Z Takacs: "Test surfaces useful for calibration of surface profilometers," United States Patent No.: 8,616,044.

[2] V. V. Yashchuk, E. H. Anderson, S. K. Barber, N. Bouet, R. Cambie, R. Conley, W. R. McKinney, P. Z. Takacs, D. L. Voronov, "Calibration of the modulation transfer function of surface profilometers with binary pseudo-random test standards: expanding the application range to Fizeau interferometers and electron microscopes," Opt. Eng. 50(9), 093604 (2011); doi:10.1117/1.3622485.

[3] V. V. Yashchuk, R. Conley, E. H. Anderson, S. K. Barber, N. Bouet, W. R. McKinney, P. Z. Takacs, D. L. Voronov, "Characterization of electron microscopes with binary pseudo-random multilayer test samples," Nucl. Instr. and Meth. A 649(1), 150-152 (2011); doi: 10.1016/j.nima.2010.11.124.

[4] V. V. Yashchuk, P. J. Fischer, E. R. Chan, R. Conley, W. R. McKinney, N. A. Artemiev, N. Bouet, S. Cabrini, G. Calafiore, I. Lacey, C. Peroz, and S. Babin, "Binary pseudo-random patterned structures for modulation transfer function calibration and resolution characterization of a full-field transmission soft x-ray microscope," Rev. Sci. Instrum. 86(12), 123702/1-12 (2015); doi: 10.1063/1.4936752.

[5] S. Babin, N. Bouet, S. Cabrini, G. Calafiore, R. Conley, G. Gevorkyan, K. Munechika, A. Vladár, and V. V. Yashchuk, "1.5 nm fabrication of test patterns for characterization of metrological systems," Proc. SPIE 10145, 1014518/1-9 (2017); doi:10.1117/12.2257624.

[6] V. V. Yashchuk, N. A. Artemiev, I. Lacey, W. R. McKinney, and H. A. Padmore, "A new X-ray optics laboratory (XROL) at the ALS: Mission, arrangement, metrology capabilities, performance, and future plans," Proc. SPIE 9206, 92060I/1-19 (2014); doi:10.1117/12.2062042.

[7] V. V. Yashchuk, N. A. Artemiev, I. Lacey, W. R. McKinney, and H. A. Padmore, "Advanced environmental control as a key component in the development of ultra-high accuracy ex situ metrology for x-ray optics," Opt. Eng. 54(10), 104104/1-14 (2015); doi: 10.1117/1.OE.54.10.104104.

[8] E. E. Fenimore and T. M. Cannon, "Coded aperture imaging with uniformly redundant arrays," Appl. Opt. 17(3), 337–347 (1978).

[9] E. Caroli, J. B. Stephen, G. Di Cocco, L. Natalucci, and A. Spizzichino, "Coded aperture imaging in x- and gamma-ray astronomy," Space Sci. Rev. 45, 349–403 (1987).